Enhanced Photovoltaic Performance of TiO₂ Dye-Sensitized Solar Cell Based on One-Dimensional Composite Photoanode

Zhangkai He[1], Jing Li[1], Duofa Wang[1,2,3,], Jinzhao Wang[3] and Tianjin Zhang[1,2,3,*]*

[1] Hubei Collaborative Innovation Center for Advanced Organic Chemical Materials,
Hubei University, Wuhan 430062, People's Republic of China
[2] Key Laboratory for the Green Preparation and Application of Functional Materials, Ministry of Education, Hubei University, Wuhan 430062, People's Republic of China
[3] School of Material Science and Engineering, Hubei University, Wuhan 430062, People's Republic of China
[*] E-mail: wangdf@hubu.edu.cn, zhangtj@hubu.edu.cn
Zhangkai He and Jing Li contribute equally to this paper.

We fabricated dye-sensitized solar cells (DSSCs) with photoanodes based on small TiO₂ nanorods (80 nm in length, 15 nm in diameter).These nanorods had a comparable specific surface area to that of spherical nanoparticles but showed superior electron transfer properties. We found that the nanorod based DSSCs showed high photoelectron conversion efficiencies. To further improve the cell performance we attempted to increase the dye adsorption and electron transfer efficiency with bi- and trilayered composite photoanode structures, fabricated by stacking layers of TiO₂ nanorods and nanotubes. The cells with a multilayer structure showed markedly higher conversion efficiency. The bilayer composite photoanode solar cell exhibited an efficiency of 7.39%, which was much higher than that of the monolayer (6.30%). A sandwiched trilayer structure showed the highest efficiency of 8.31%. Electrochemical impedance spectroscopy showed that the improvement in efficiency could be attributed to enhanced electron transport.

Keywords: dye-sensitized solar cells; composite photoanode; TiO₂

1. INTRODUCTION

Dye-sensitized solar cells (DSSCs) have emerged as attractive candidate devices for harnessing solar power, owing to their potentially low costs of production and relatively high energy conversion efficiencies [1-2]. As a main component of DSSCs, the photoanode acts as a substrate that dye molecules can adsorb to and also provides an electron transport channel. An efficient photoanode

should have a sufficiently high surface area to give good dye adsorption, efficient electron transfer, and effective light harvesting. Over recent years, TiO_2 spherical nanoparticles (NPs) have been widely used in DSSCs because of their low cost, low toxicity, and high specific surface areas [3-5]. However, electron transport in TiO_2 NP films takes place in a random manner, which causes deterioration of device performance from electron-hole recombination process [6]. One-dimensional structured TiO_2 nanotube (NT) and nanorod (NR) based devices have been developed owing to their efficient charge transfer abilities [7-9]. These NRs and NTs are typically prepared by hydrothermal or electrochemical methods and their diameters are greater than 100 nm. However, the number of sites for dye adsorption in these materials is relatively limited compared with that in NP layers. Thus, the photoelectron conversion efficiency (PCE) of devices based on NRs and NTs is often lower. Recently, Marco reported the successful fabrication of small TiO_2 NRs (5 nm $\times$30 nm) by a modified solvothermal method. The small NRs showed surface areas comparable to those of NPs, but also featured superior electron transfer performance. Therefore, a high DSSC PCE of 7.9% was achieved [9].

More recently, composite-structured photoanodes based on hierarchical nanostructures and multiple layers have been reported as an effective method for providing a high surface area and efficient electron transfer [10-14]. Lee explored a TiO_2 NP/NR composite film photoanode, which combined the high specific surface area of NPs and efficient electron transport of NRs [15]. Wu and co-workers designed a multi-stack integrated three-dimensional hyperbranched anatase architecture composed of hierarchical tree-like nanowires and sub-micrometer spheres. In the hyper architectures, efficient dye adsorption and charge collection from the hierarchical nanowires and strong light harvesting by the sub-micrometer spheres was realized to achieve a high PCE of 11.0% [16]. However, the preparation of these three-dimensional hyperbranched architectures was rather complicated and is not applicable for commercialization. Yun reported a bilayer photoanode DSSC based on stacking of TiO_2 NPs on NTs. Cells with this bilayer structure showed an efficiency of 7.2%, which was considerably higher than that of single layer cells. In this case the enhanced efficiency was attributed to efficient charge collection [17].

In the present study, we report a composite photoanode based on stacking of small NRs and NTs. The small NRs had a surface area comparable to that of NPs but also showed superior electron transfer properties. Accordingly, the NR based DSSC showed better photovoltaic performance. Integration of small NRs with NTs further improved the dye adsorption and electron transfer efficiency, leading to power conversion efficiencies as high as 8.31%.

2. EXPERIMENTAL

The NR and NP photoanode fluorine doped tin oxide (FTO) substrates were prepared by a doctor blade method (with a paste purchased form Wuhan lattice solar energy co., Ltd). The nNR (n=2-5) photoanode was obtained by repeating the doctor blade process. For the NR/NT, 2NR/NT, NR/NT/NR composite photoanode, a TiO_2 NT array for use in the over-layer was first prepared by a two-step anodization process with Ti foil. The NTs were then transferred onto the NR sublayer [18,19]. Dye adsorption was achieved by immersing the TiO_2 photoanode in a 0.3 mM N719 dye

solution for 24 h. The electrolyte contained 0.3 M LiI, 0.05 M I_2, 0.6 M 1-propyl-3-methylimidazolium iodide and 0.5 M tert-butylpyridine in dry acetonitrile. A platinum counter electrode was used for the cell.

X-ray diffraction (XRD) patterns were recorded using a Rigaku D/MAX-3A X-ray diffractometer with Cu Ka radiation (k=0.15406 nm) at a scan rate of 5°/min. The morphology of the layers was imaged with a JSM-6510LV scanning electron microscopy (SEM, JEOL). Transmission electron microscope (TEM) analysis was performed with a JEM-2100F electron microscope (JEOL, Japan) at an accelerating voltage of 200 kV. The photocurrent density-voltage (*J-V*) curves of the assembled DSSCs were recorded by a Keithley 2400 Sourcemeter with simulated AM1.5 sunlight with an output power of 100mW/cm^2 produced by a solar simulator (Newport 91192). Electrochemical impedance spectroscopy (EIS) measurements were performed at the open-circuit voltage of each DSSC under light illumination with an AutoLab (IM6, Zahner).

3. RESULTS AND DISCUSSION

The crystalline structure of the monolayer and the composite photoanode were characterized by XRD measurements as shown in Fig. 1.
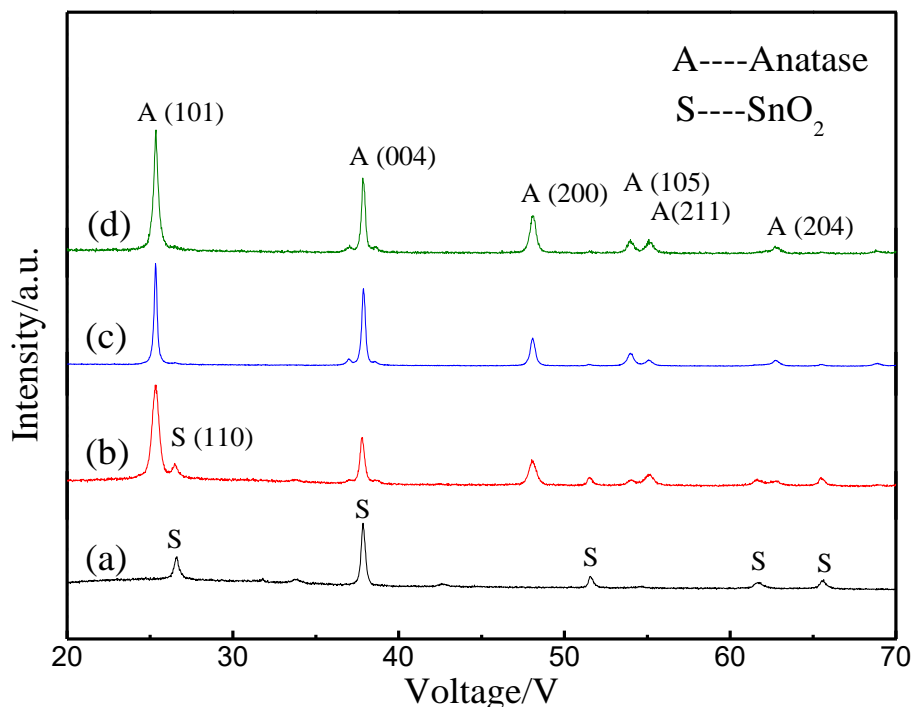
Figure 1. X-ray diffraction patterns of (a) FTO substrate, (b) NR film on an FTO substrate, (c) bilayer film (NR/NT), (d) trilayer film (NR/NT/NR). Structures of the bi- and trilayer photoanode films (as illustrated in Figure.5).

In the XRD spectra, well-defined diffraction peaks at 25.35°, 37.84°, 48.14°, 53.97°, 55.18°, and 62.81° were observed, which were attributed to the (101), (004), (200), (105), (211), and (204) crystal planes of anatase TiO_2 [20]. Diffraction peaks from SnO_2 were also observed from the FTO substrate [21]. The XRD results indicated that the TiO_2 NRs and NTs were highly crystalline.
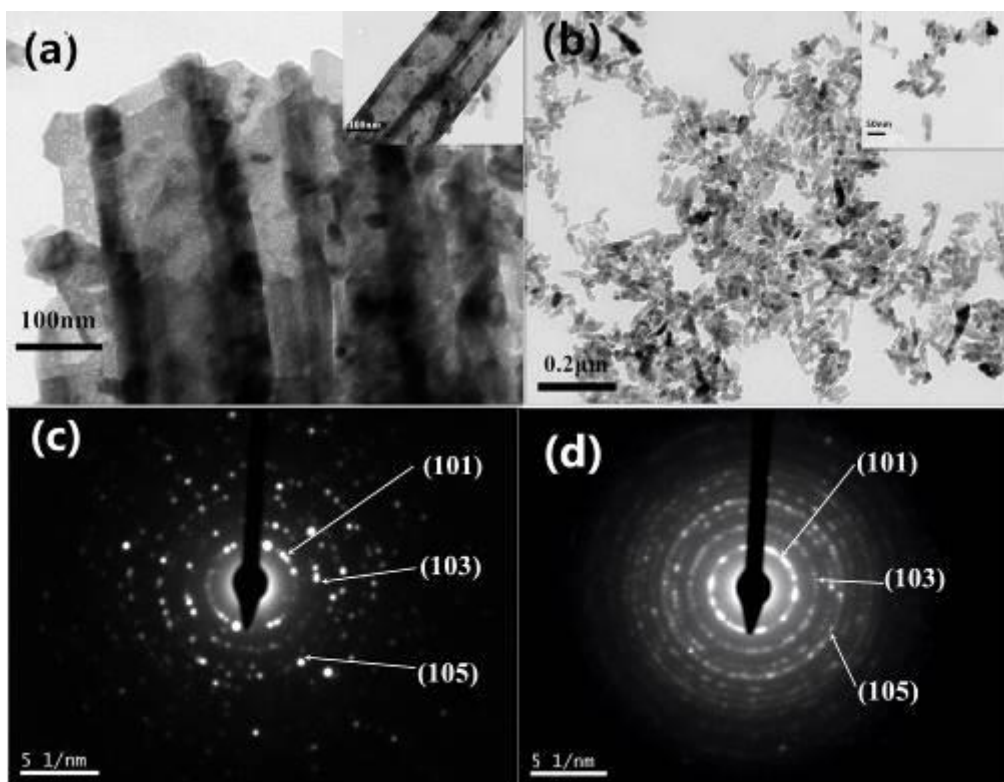
Figure 2. TEM images of the (a) NTs and (b) NRs, SAED pattern of (c) an NT and (d) NRs.

The TEM images and selected-area electron-diffraction (SAED) patterns of the NRs and NTs are shown in Fig. 2. These images clearly showed the morphology of the NRs and NTs, the length and diameter of the NRs were 80and 15 nm, respectively. The thickness and pore diameters of the NTs were about 15 and 90 nm, respectively. The SAED patterns indicated that the TiO_2 NRs and NTs were polycrystalline [19,21]. The diffraction rings could all be indexed to specific planes of anatase phase of TiO_2, as indicated in the figure. These results were also consistent with the XRD findings shown in Fig. 1.

The photovoltaic performance of the NP and small NR based DSSCs were characterized. Current density-voltage (*J-V*) curves are shown in Fig.3. The NR based DSSCs had better photovoltaic performance than those based on NPs. At the same thickness, the NR based DSSCs showed much higher conversion efficiency. Considering that the dye adsorption ability of the NPs and NRs was similar, the higher photovoltaic performance of the NR based cells was attributed to improved electron transfer properties.
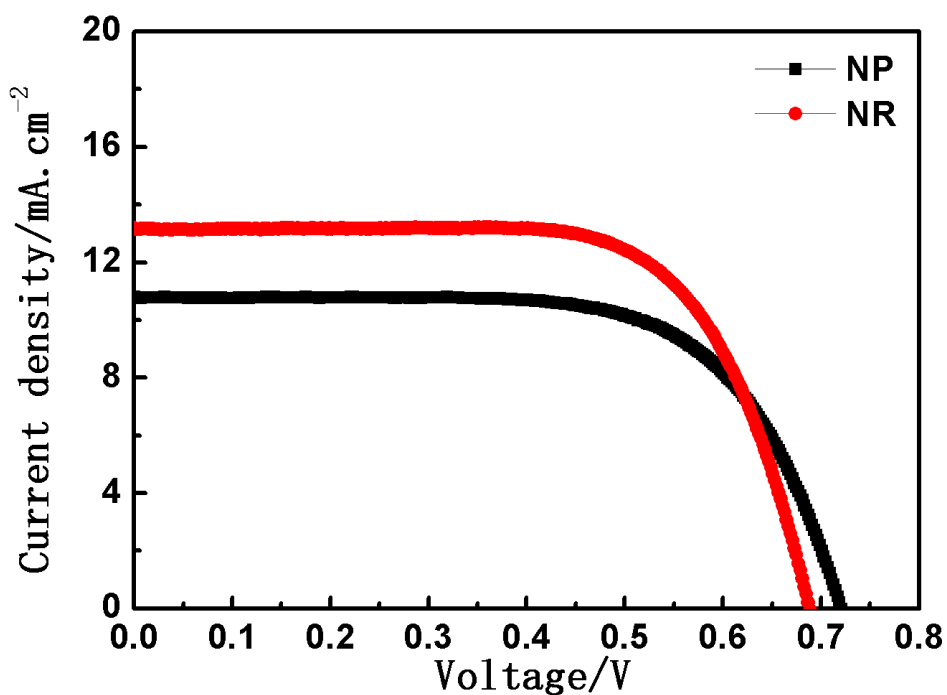
Figure 3. *J-V* curves of the DSSCs with NP and NR photoanodes.
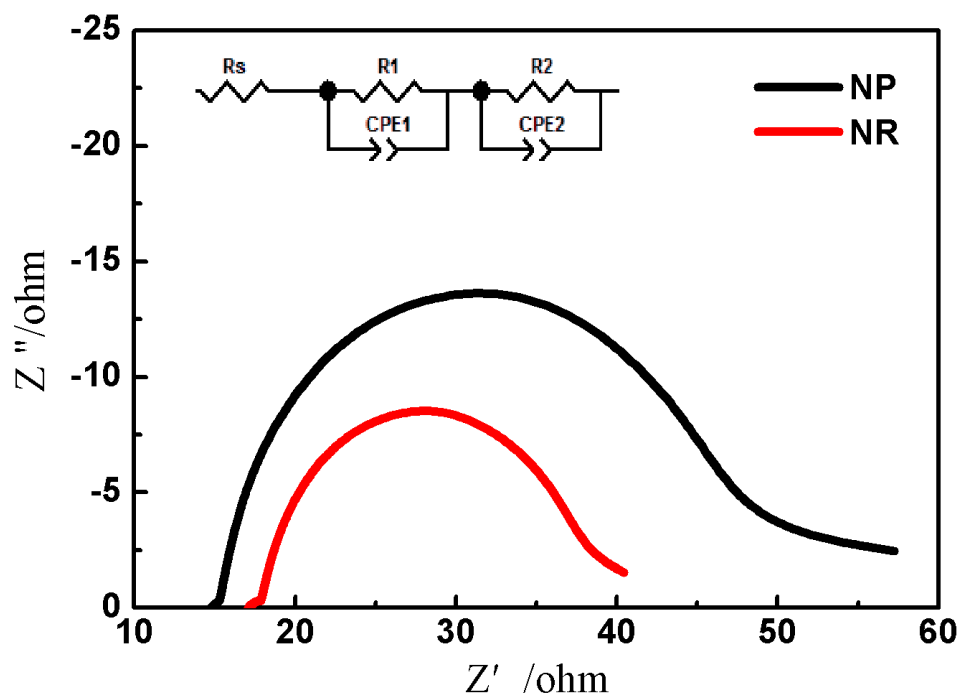
Figure 4. Nyquist plots of the EIS performed on DSSCs with NP and NR photoanodes.

To reveal differences in the charge transfer phenomena of the NR and NP cells, we used electrochemical impedance spectroscopy (EIS). EIS is an effective technique for investigating charge-transport phenomena in DSSC. Figure 4 shows the EIS spectra measured under AM 1.5 sunlight illumination at a potential corresponding to the open-circuit voltage. Nyquist plots for DSSCs generally exhibit three semicircles, however, only two semicircles were observed in the present study due to the low resistance of ion transport in the electrolyte. The semicircle in the high-frequency region was attributed to the charge transfer resistance (R_1) at the platinum counter electrode/electrolyte interface and the semicircle in the mid-frequency region was attributed to electron transfer and transport resistance (R_2) at the TiO_2/dye/electrolyte interface [22-25]. The sheet resistance, which includes contributions from the FTO glass current collector, was denoted as R_s. The equivalent circuit is shown in the inset of Fig.4. Generally, a larger radius corresponds to a higher interfacial resistance and greater current loss, therefore the charge transfer and recombination situation at the TiO_2/dye/electrolyte interface determined the shape of the semicircle in the mid-frequency region. The NR DSSCs showed lower charge transfer resistance than that of the NP based DSSCs. This observation was in accordance with the higher photovoltaic efficiency. The TiO_2 NRs promoted photo generated charge transfer and decreased the charge recombination rate, which in turn enhanced the photovoltaic performance.

To further increase the dye adsorption, we tried to increase the thickness of the NR layer. The thickness dependent photovoltaic properties of our NR DSSCs are listed in Table 1. The conversion efficiency did not increase linearly with the thickness of the NR layer. When the NR layer was thicker than 14.5 μm the efficiency started to decline. As the thickness of a photoanode layer is increased, the amount of dye incorporated into the film also increases, however, the probability of electron recombination also increases owing to the longer distance to the collection electrode. Therefore, the conversion efficiency reaches a maximum value at a certain optimum photoanode layer thickness.

Table 1. Photovoltaic characterization of NR based DSSCs with different NR layer thicknesses. Numbers before "NR" denote the number of layers applied during the doctor blade process.

Sample	Thickness	J_{sc} (mA/cm^2)	V_{oc} (mV)	FF	η
NR	7.2 μm	13.2	0.688	72.4 %	6.58 %
2NR	11.1μm	13.8	0.674	69.9 %	6.49 %
3NR	14.5 μm	13.7	0.675	69.8 %	6.43 %
4NR	19.4 μm	14.0	0.665	67.0 %	6.28 %
5NR	23.1 μm	14.1	0.639	70.3 %	6.29 %

FF: fill factor; η: photoelectric conversion efficiency；J_{sc}: short-circuit current density; V_{oc}: open-circuit voltage.

To improve dye adsorption without adversely affecting electron transport, we fabricated composite photoanodes with NRs and NTs. We used the small NRs described above and NTs prepared

by an electrochemical anodization method. We fabricated three different composite photoanodes as illustrated in Fig. 5.

NR/NT   2NR/NT   NR/NT/NR
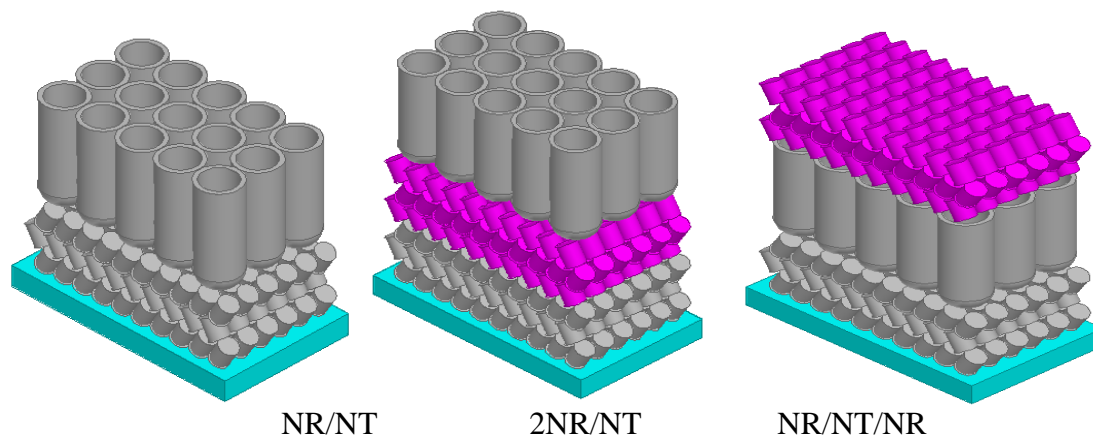
Figure 5. Schematic diagrams of composite photoanodes with different structures.
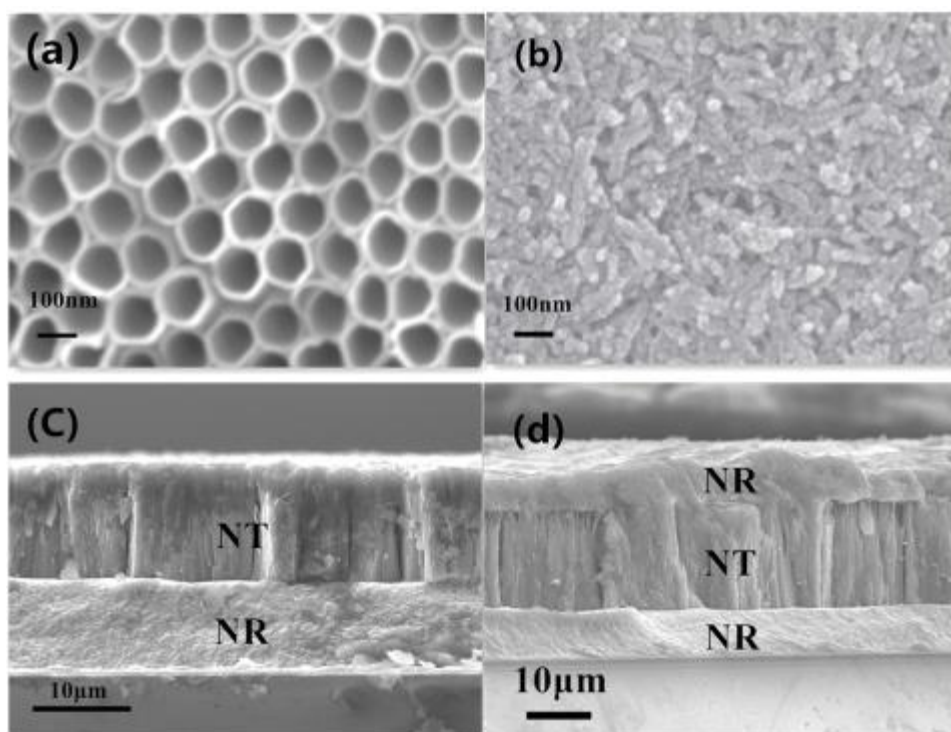
Figure 6. Top view SEM images of (a) NTs and (b) NRs, (c) side view SEM images of NR/NT and (d) NR/NT/NR based TiO_2 composite photoanodes.

To ensure good connection between the NR and NT layers, the composite photoanode was annealed at 500 °C for 30 min after the NT layer was coated on top of the NR layer. For the sandwiched NR/NT/NR structure, the top nanorod layer was deposited by a doctor blade method directly after the NT layer was deposited. After the final NR layer was deposited the whole sample was annealed at 500 °C. The 2NR/NT structure was achieved by doubling the NR layer thickness.
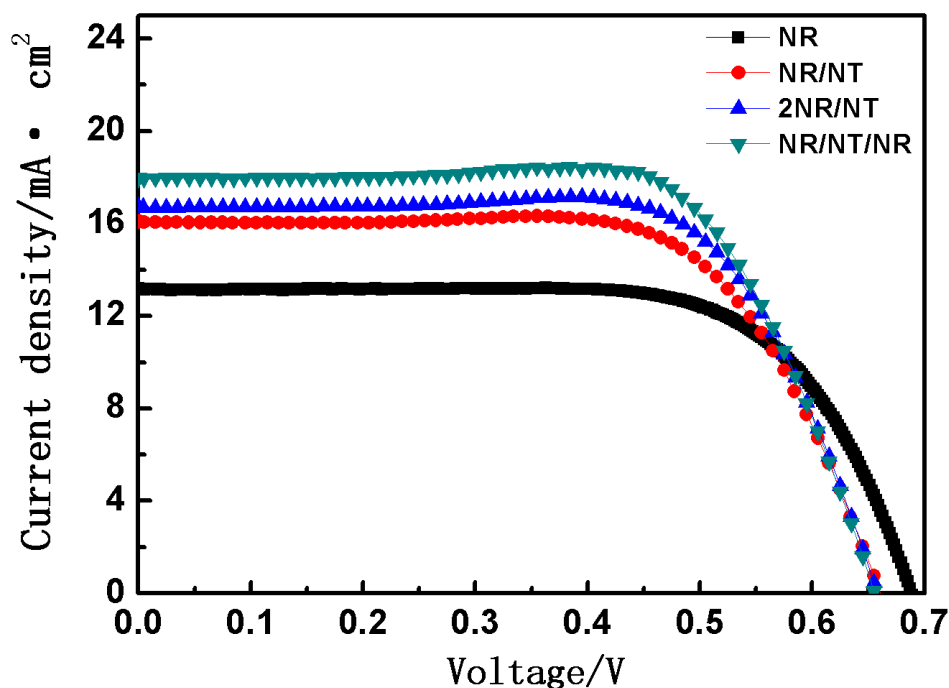
Figure 7. *J-V* curves of the DSSCs with different photoanodes.

The morphology of these composite photoanodes was imaged by SEM, as shown in Fig 6. Top view SEM images showed that layers of NTs and porous NRs were successfully fabricated. The thickness and pore diameters of the NTs were about 15 and 90 nm, respectively. From side view images, the bi- and trilayer structures could be clearly observed. The interface between the layers was clean and the contacts appeared to be good.

The *J-V* characteristics of DSSCs based on these layered structures are shown in Fig. 7. The details of the photovoltaic performance, such as J_{sc}, V_{oc}, FF, PCE are summarized in Table 2.

Table 2. Photovoltaic characterization of composite DSSCs with different structures.

Sample	$J_{sc}(mA/cm^2)$	$V_{oc}(mV)$	FF	η	AD (mol/cm^2)
NR	13.2	0.688	72.4 %	6.58 %	1.79×10^{-7}
NR/NT	16.0	0.659	70.1 %	7.39 %	1.91×10^{-7}
2NR/NT	16.7	0.657	70.5 %	7.74 %	4.22×10^{-7}
NR/NT/NR	18.0	0.655	70.5 %	8.31 %	4.11×10^{-7}

η = photoelectric conversion efficiency, AD=Amount of dye absorption.

For comparison, the results from a DSSC with a single layer photoanode are also included in the table. The composite photoanode structures effectively boosted the PCE of these DSSCs. The NR/NT bilayer DSSC showed a PCE of 7.39 %, with a J_{sc} of 16.0 mA/cm^2, a V_{oc} of 0.659 V, and a FF of 70.1%. These values were all higher than those measured for the single layer NR based cell. When

the 2NR/NT photoanode was used, the conversion efficiency reached 7.74%, which was slightly higher than that of the NR/NT cell. However, when the NT layer was sandwiched between top and bottom NR layers, namely the NR/NT/NR structure, the PCE markedly increased to 8.31%, with a J_{sc} of 18.0 mA/cm^2, a V_{oc} of 0.655 V, and a FF of 70.5%. Clearly the stacking sequence affected the photovoltaic performance of the DSSC. The PCE is higher than most of the literature reports with the multilayed composite photoanode DSSC [15, 23, 27-29]. The tri-layer structure appears to be an more efficient DSSC photoanode than the bi-layer structure which is most widely used in the composite photoanode. Another important factor is ascribed to the utilization of small nanorod. It exhibits comparable dyes adsorption ability but more efficient electron transport compare with the nanoparticle. We next investigated the amount of dye adsorption. The dye content of the film increased in proportion to the film thickness. The amount of dye absorption was calculated by Beer's law according to previous reports and these data are listed in Table 2 [26]. Compared with the single layer photoanode DSSC, the composite DSSC contained more dyes. In particular, the trilayer DSSC had around three times as much dye as the single layer device. The larger amount of dye increased the light absorbance of the cells and contributed to the enhanced photovoltaic performance of the composite DSSCs. However, when the 2NR/NT and NR/NT/NR DSSC were compared, the 2NR/NT had lower PCE, but showed a larger amount of dye adsorption in the film. The superior photovoltaic performance of the NR/NT/NR DSSC cannot be explained simply by dyes adsorption.

We used EIS analysis to investigate the electron transport properties of the DSSC with different composite structures. The EIS was measured under AM 1.5 light illumination at an applied bias of V_{oc}, as shown in Fig. 8.
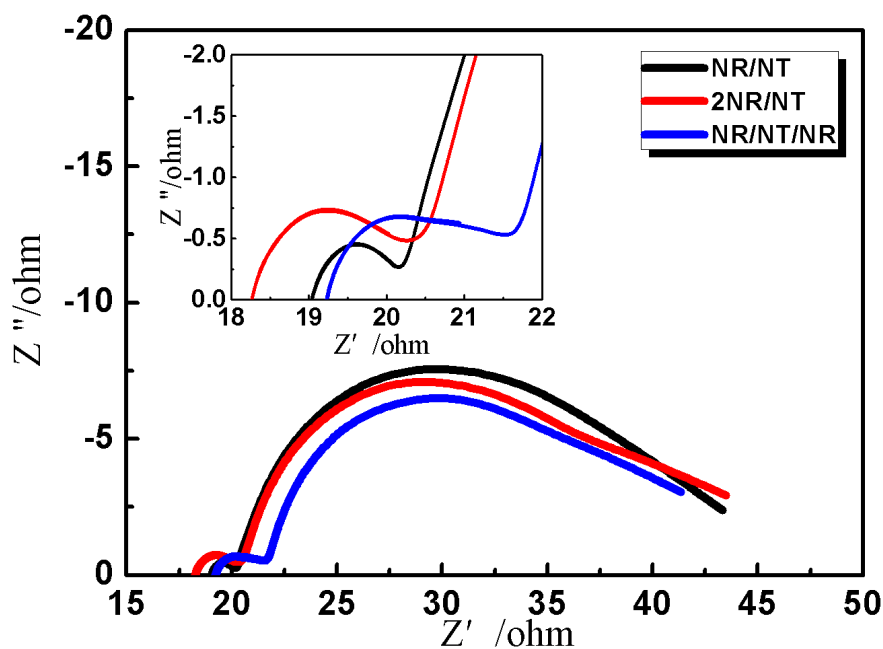
Figure 8. Nyquist plots of EIS performed on the DSSCs with different composite TiO$_2$ photoanodes.

We fitted the EIS data using the equivalent circuit shown in the inset of Fig. 4. Table 3 plots the values of R_s, R_1, R_2, and the electron lifetime (τ). We deduced τ using the equation $\omega\tau=1$ [23]. The bi- and trilayer structured DSSCs had a smaller charge transfer resistance at the TiO_2/dye/electrolyte interface (R_2) and a longer electron lifetime than those of the single layer NR and NP based devices. The decrease in R_2 was the result of a higher electron injection rate from the lowest unoccupied molecular orbit of the dye molecules into the TiO_2 conduction band, owing to the greater dye adsorption[30, 31].

Table 3. Resistance of DSSCs calculated from EIS data.

Sample	$R_s (\Omega)$	$R_1 (\Omega)$	$R_2 (\Omega)$	τ (ms)
NP	14.78	0.55	33.44	25.75
NR	15.80	0.64	25.77	38.93
NR/NT	19.02	1.16	19.48	56.46
2NR/NT	18.28	1.95	17.95	62.66
NR/NT/NR	19.23	2.32	16.70	65.83

This lower charge transfer resistance R_2 improved the PCE of the composite photoanode cells. When the two trilayer structures were compared, the NR/NT/NR cell showed a smaller charge transfer resistance R_2 at the TiO_2/dye/electrolyte interface than that of the 2NR/NT DSSC. The NTs of the sandwich structure likely acted as an efficient electron transport channel between the top and bottom NR layers. This may explain the anomalously high PCE of the NR/NT/NR structured DSSCs.

4 CONCLUSIONS

We fabricated DSSCs using small NRs (80 nm long and 15 nm wide), which had a specific surface area comparable to that of NPs, but superior electron transfer properties. The NR based DSSCs showed high photovoltaic performance. To further improve the dyes adsorption and electron transfer efficiency, we fabricated bi- and trilayered composite photoanodes with different structures by stacking TiO_2 NRs and NTs. The multilayer photoanode structures clearly enhanced the PCEs of their respective DSSCs. The bilayer composite photoanode DSSC exhibited a PCE of 7.39%, which was much higher than the monolayer efficiency of 6.30%. The sandwiched trilayer structure showed the highest PCE of 8.31%. EIS measurements indicated that the improvement of PCE could be mainly attributed to enhanced electron transport efficiency.

References

1. B. O'regan, M.Grätzel, *Nature.*, 737 (1991) 353.
2. M. Grätzel, *J. Photochem. and Photobiol. C: Photochem. Rev.*, 4 (2003) 145-153.
3. D. Sengupta, P. Das, B. Mondal, and K. Mukherjee, *Renewable sustainable Energy Rev.*,60 (2016) 356.
4. Y. Ding, L. Zhou, L. Mo, L Hu, and Z Li, *Adv. Func. Mater.*, 25 (2015) 5946.
5. P. S. Shen, C. M. Tseng, T. C. Kuo, C. K Shih, M. H. Li, and P. Chen, *Sol. Energy.*, 120 (2015) 345.
6. J. H. Yang, C.W. Bark, K. H. Kim, and H. W. Choi, *Jpn. J. Appl. Phys.*, 53 (2014) 11RB02.
7. Z. Hou, W. Que, J. Ren, Y. Xing, H. M . A. Javed, T. Zhou, and L. B. Kong, *Ceram. Int.*, 41 (2015) S719.
8. Z. Jing, B. Yang, Z. Kun, L. Ye, and K. Lu, *Ceram. Int.*, 41 (2015) 7235.
9. L. DeMarco, M. Manca, R. Giannuzzi, F. Malara, G. Melcarne, G. Ciccarella, I. Zama, R. Cingolani, and G. Gigli, *J. Phys. Chem. C.*, 114 (2010) 4228.
10. J. Akilavasan, M. Al-Jassim, and J. Bandara, *J. Nanophoton.*, 9 (2015) 093091.
11. W. Q. Wu, Y. F Xu, H. S. Rao, and D. B. Kuang, *J. Phys. Chem.* C, 118 (2014) 16426.
12. W. Q. Wu, B. X. Lei, H. S. Rao, Y. F. Xu, Y. F. Wang, and C. Y. Su, *Sci. Rep.*, 3 (2013) 1352.
13. W. Q. Wu, Y. F. Xu, C. Y. Su, and D. B. Kuang, *Energy Environ. Sci.*, 7 (2014) 644.
14. W. Q. Wu, Y. F. Xu, H. S. Rao, C. Y. Su, and D. B. Kuang, *Angew. Chem. Int. Ed.*,53 (2014) 4816.
15. K. W. Lee, M. Kim, J. M. Kim, J. J. Kim, and I. H. Lee, *J. Alloys Compd.*, 656 (2016) 568.
16. W. Q. Wu, Y. F. Xu, H. S. Rao, and D. B. Kuang, *J. Am. Chem. Soc.*,   136 (2014) 6437.
17. H. G. Yun, J. H. Park, B. S. Bae, and M. G. Kuang, *J. Mater. Chem.*, 21 (2011) 3558.
18. M. M. Momeni and M. G. Hosseini, *J Mater. Sci.: Mater Electron.*, 25 (2014) 5027.
19. Z. Su, L. Zhang, F. Jiang, and M. Hong, Prog. *Nat. Sci.: Mater. Inter.*, 23 (2013) 294.
20. S.Kathirvel, C. Su, H. C. Lin, B. R. Chen, and W. R. Li, *Mater. Lett.*, 129 (2014) 149.
21. S. Kathirvel, C. Su, C. Y. Yang, Y. J. Shao, B. R. Chen, and W. R. Li, *Vacuum*,118 (2015) 17.
22. A. Subramanian and H. W. Wang, *J. Photochem. Photobiol. A: Chem.*, 279 (2014) 32.
23. M. A. Hossain, J. Park, J. Y. Ahnet, C. Park, Y. Kim, S. H. Kim, and D. Li, *Electrochem. Acta.*, 173 (2015) 665.
24. T. S. Eom, K. H. Kim, C. W. Bark, and H. W. Choi, *J. nanosc. nanotech.*, 14 (2014) 7705.
25. Y. Cao, Y. J. Dong, H. L. Feng, H. Y. Chen, and D. B. Kuang, *Electrochem. Acta.*, 189 (2016) 259.
26. D. S. Tsoukleris, I. M. Arabatzis, E. Chatzivasiloglou, A. I. Kontos, V. Belessi, M. C. Bernard, and P. Falaras, *Solar Energy.*, 79 (2005) 422.
27. H. Yun, J. H. Park, B. Bae, and M. G. Kang, *J. Mater. Chem.*, 21 (2011) 3558.
28. X. Xin, J. Wang, W. Han,M. Ye, and Zhiqun Lin, *Nanoscale*, 4 (2012) 964.
29. G. Wang, W. Xiao, and J. Yu, *Energy*, 86 (2015) 196.
30. C. P. Hsu, K. M. Lee, J. T. W Huang, C. H. Lee, L. P. Wang, S.Y. Tsaic, and K.C. Ho, *Electrochem. Acta.*, 53 (2008) 7514.
31. K. M. Lee, V. Suryanarayanan, and K. C. Ho, *J. Power Sources.*, 188 (2009) 635.